Numerical Modeling of Arcjet Thruster: Effect of Design & Operating Parameters on Arc Heating

IEPC-2017-532

Presented at the 35th International Electric Propulsion Conference
Georgia Institute of Technology • Atlanta, Georgia • USA
October 8 – 12, 2017

Nandyala Hari Prasad[1] Amit Kumar[2] and T Jayachandran[3]
Department of Aerospace Engineering, Indian Institute of Technology Madras, India

P Peeraiah[4]
Vikram Sarabhai Space Centre, Indian Space Research Organization, Thiruvananthapuram, India

Abstract: Arcjet thrusters are space electric propulsion systems that are being adopted for use in modern satellites for station keeping and attitude control. These thrusters are classified as electro-thermal based operating principle of heating propellants by electrical arcs. In the present work a 2D axisymmetric CFD computer program (in FORTRAN) was developed to simulate arcjet flow physics for better understanding and design of the device. The CFD code was successfully tested to simulate arcjet thrusters from literature. Subsequently the code was used to simulate 0.1 N class radiatively cooled hydrazine arcjet. A parametric study was carried to study effect of geometrical parameters on arc heating.

Nomenclature

r, z, θ	=	radial, axial and azimuthal coordinates
$\boldsymbol{V}$	=	velocity vector
v_r, v_z	=	radial and axial components of velocity vector
ρ	=	density
T	=	Gas Temperature
e_t	=	Total energy
p	=	Pressure
$\bar{\bar{\boldsymbol{\tau}}}$	=	Viscous stress tensor
R_{gas}	=	Characteristic gas constant
μ	=	Coefficient of viscosity
K	=	Thermal conductivity
I	=	electric current
$\boldsymbol{J}$	=	current density vector
j_r, j_z	=	radial and axial components of current density vector
$\boldsymbol{E}$	=	electric field vector
E_r, E_z	=	radial and axial components of electric field vector
$\boldsymbol{B}$	=	magnetic induction vector
B_θ	=	azimuthal component of magnetic induction vector
σ	=	electrical conductivity

[1] PhD research scholar, hari25.astro@gmail.com.
[2] professor, amitk@ae.iitm.ac.in
[3] visiting faculty (formally deputy director VSSC)
[4] scientist

I. Introduction

At present the space propulsion systems in almost all the Indian satellites for station keeping and attitude control are of chemical type such as ones using hydrazine monopropellant. To increase the life of satellites there is move towards using electric propulsion based thrusters owing to the higher specific impulse possible with these systems compared to chemical systems. The exhaust velocity of a chemical thruster is limited by the energy stored within the chemical bonds of the propellants. The maximum attainable exhaust velocity with practical propellants like hydrogen and oxygen is about 4500 m/s. To achieve higher exhaust velocity, larger amount of energy needs to be added to the propellant beyond the chemical bond energies. This is facilitated in an electric propulsion system where electrical energy from an external source is added to the propellants. Increased exhaust velocity results in reduced propellant weight thus increase payload and /or increased life of the satellite. One possible extension of chemical system to electric propulsion system is hydrazine arcjet where decomposing hydrazine is heated further by an electric arc to augment the thruster performance. Although arcjets and other electric propulsion systems were conceived in 1950's the weight of power source per unit power and conversion efficiencies were low. With the improvement in these there is renewed interest in such systems for space application all over the world. There is vast literature on arcjet experiments [1] and modeling [2-7], however, the design features and parameters of an arcjet are primarily from experience. A proper understanding of flow physics of these devises will help improve design and thus their performance. In view of this a 2D axisymmetric numerical model is developed to simulate radiatively cooled hydrazine arcjet thruster. The model is validated and used to carry out parametric study on various design parameters and input current. A typical arcjet thruster geometry described in terms of constrictor length (L_c) is shown in Fig.1.

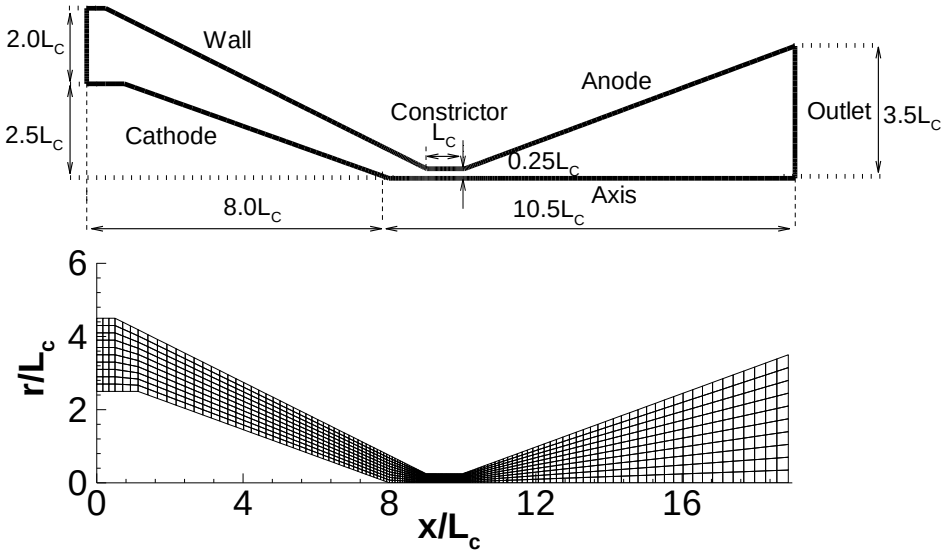

Figure.1 Schematic of a arcjet thruster in base dimensions scaled with constrictor length showing computational domain (upper) and computational mesh (lower)

II. Numerical Modelling

A. Governing Equations

The plasma flow in the thruster is modelled following some simplifying assumptions and using governing equations based on conservation laws and thermodynamics to simulate important physical processes in the thruster. The key assumptions of the model are outlined below.

1) Plasma flow in the Arcjet nozzle is steady, axisymmetric, laminar and compressible.
2) Plasma is optically thin and in the Local Thermodynamic Equilibrium (LTE) state, thus the thermodynamic and transport properties are determined by the local gas temperature and pressure.
3) Swirling velocity is negligible in comparison with axial velocity.
4) Radiation heat transfer and electrical sheath formation at solid boundaries are not considered.

5) Displacement current in Ampere's law is neglected due to its smaller magnitude compared to conduction current.

The performance prediction of an Arcjet thruster is accomplished by solving integral form of governing equations for compressible flow which comprise of mass conservation, momentum (including viscous term) and energy conservation (includes thermal diffusion) equations with the electromagnetic body forces and Joule (Ohmic) heating included as source terms in momentum and energy equations. Maxwell's equations for steady state together with Ohm's law and Ampere's law are used to determine magnetic field and current density. The above stated governing equations in cylindrical coordinates (r, z) can be written as follows

$$\frac{\partial}{\partial t}\oint \rho \, d\Omega + \oint \rho \boldsymbol{V} \cdot \boldsymbol{n} ds = 0 \tag{1}$$

$$\frac{\partial}{\partial t}\oint \rho \boldsymbol{V} d\Omega + \oint \rho \boldsymbol{V} \cdot \boldsymbol{V} \cdot \boldsymbol{n} \boldsymbol{ds} = -\oint P \, \boldsymbol{n} ds - \oint \bar{\bar{\boldsymbol{\tau}}} \cdot \boldsymbol{n} \boldsymbol{ds} + \oint \mathbf{J} \times \mathbf{B} \, d\Omega \tag{2}$$

$$\frac{\partial}{\partial t}\oint \rho \, e_{\boldsymbol{t}} d\Omega + \oint (\rho e_{\boldsymbol{t}} + P)\boldsymbol{V} \cdot \boldsymbol{n} \boldsymbol{ds} = -\oint (\boldsymbol{q} \cdot \boldsymbol{n}) ds + \oint \mathbf{J} \cdot \mathbf{E} \, d\Omega \tag{3}$$

$$\tau_{rr} = 2\mu\left(\frac{\partial v_r}{\partial r} - \frac{1}{3}\boldsymbol{\nabla} \cdot \boldsymbol{V}\right) \qquad \tau_{zz} = 2\mu\left(\frac{\partial v_z}{\partial z} - \frac{1}{3}\boldsymbol{\nabla} \cdot \boldsymbol{V}\right) \qquad \tau_{\theta\theta} = 2\mu\left(\frac{v_r}{r} - \frac{1}{3}\boldsymbol{\nabla} \cdot \boldsymbol{V}\right) \qquad \tau_{rz} = \mu\left(\frac{\partial v_r}{\partial z} + \frac{\partial v_z}{\partial r}\right) \tag{4}$$

$$q_z = v_z \tau_{zz} + v_r \tau_{rz} + K\frac{\partial T}{\partial z} \qquad q_r = v_z \tau_{rz} + v_r \tau_{rz} + K\frac{\partial T}{\partial r} \tag{5}$$

$$\boldsymbol{J} = \sigma(\boldsymbol{E} + \boldsymbol{V} \times \boldsymbol{B}) \tag{6}$$

$$\frac{\partial}{\partial z}\left[\frac{1}{r \cdot \sigma}\frac{\partial (rB_\theta)}{\partial z}\right] + \frac{\partial}{\partial r}\left[\frac{1}{r \cdot \sigma}\frac{\partial (rB_\theta)}{\partial r}\right] = \mu_0\left[\frac{\partial (v_z B_\theta)}{\partial z} + \frac{\partial (v_r B_\theta)}{\partial r}\right] \tag{7}$$

B. Boundary Conditions

Boundary conditions need to be specified for Eq. (1-3) and (7), to complete the problem formulation. No-slip boundary conditions are prescribed for the velocity components, zero normal gradient of pressure is employed and Mass density is evaluated by implicit extrapolation on all solid surfaces. The radiation cooling is considered on the anode wall and adiabatic for cathode wall.

Along the centerline symmetry condition is imposed for the axial component of velocity v_z, mass density, pressure and temperature, whereas the radial component of velocity v_r is set to zero. At the inlet boundary, v_r is set to zero, and v_z is evaluated by using implicit extrapolation. At inlet by prescribing the stagnation temperature, static temperature can be evaluated once the corresponding velocity components are known .The stagnation pressure is specified at the inlet, from which the mass density can be determined once the temperature is known. At the exit plane, all the velocity components, mass density, pressure and temperature are evaluated using implicit extrapolation but if the flow is supersonic at the given point, or from a specified static pressure if the flow is subsonic at that point. Boundary conditions for the magnetic induction equation, B_θ is set to zero along the centerline (imposing symmetry on the magnetic induction at the centerline) and along the exit plane to prevent the current from blowing out of the thruster. The anode is assumed to be a perfect conductor downstream of the constrictor region, and thus the current streamlines enter the anode surface normal to it. This is imposed by setting $(\boldsymbol{\nabla} \times \boldsymbol{B}) \cdot \hat{\boldsymbol{t}} = 0$. B_θ is prescribed a value based on the total enclosed current over the first half of the constrictor wall. These conditions in effect prevent current attachment on the upstream half of the constrictor wall, and are necessary to obtain downstream arc attachment since the phenomena governing breakdown and extinction are not modeled.

C. Initial Conditions

It is extremely necessary to specify appropriate initial conditions to obtain stable solutions. For this purpose a converged cold flow solution is taken as the initial condition and the Joule heating value is incremented as the iteration progress. The specific magnitude of the values used for these initial guesses does not impact the final converged results; however, the initial profiles and magnitudes do need to be reasonable. No initial distributions are required for the magnetic induction as it is governed by an elliptic equation Eq. (7). It is important to note that since the magnetic induction equation is modeled by an elliptic equation, the burden of a good initial guess rests upon reasonable initial profiles for mass densities and temperature.

D. Properties

The transport properties are evaluated based on the pressure and temperature at corresponding grid point. The correlation for the variation of properties on pressure and temperature are obtained database [Ref murphy]. Variation of electrical conductivity with respect to temperature range above 3000K is obtained from the database. Since the database for electrical conductivity variation is not available for the colder regions of the flow (below 3000K) an exponential variation with respect to temperature is assumed. The specific value of the conductivity floor is fixed on the basis of the required input electrical power.

E. Numerical Method

The numerical model used for simulating an axisymmetric Arcjet thruster assumes local thermal equilibrium. The set of governing equations includes mass, momentum and energy conservation equations for a viscous, compressible flow with the electromagnetic body forces and Joule (Ohmic) heating as source terms in momentum and energy equations respectively. Maxwell's equations are solved together with Ohm's law (neglecting Hall Effect and ion slip), Ampere's law (neglecting displacement current) to determine magnetic field and current density. The governing equations are discretized using a cell centered finite volume method in an unstructured computational domain. For the flow equations, AUSM+-up scheme is used to compute convective fluxes. After spatial discretization the equations become ODEs in time. Then they are integrated using an explicit four-stage Runge-Kutta method. The gradient terms are computed based on Green's theorem. The steady state magnetic field equation is solved using Guass-seidel explicit scheme.

III. Results

F. Hydrazine arcjet CFD code validation

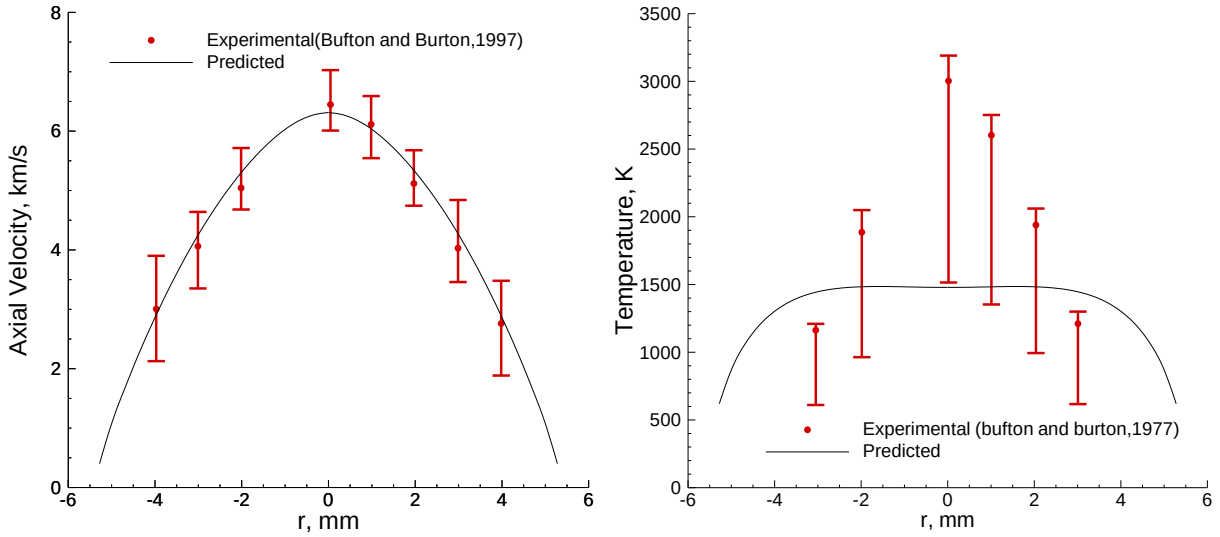

Figure 2 Comparison of predicted radial distribution at nozzle exit plane with experiments [1] for (a) axial velocity and (b) temperature.

The CFD code was developed with validation against standard compressible benchmarks like CD nozzle flow. The CFD code was then used to simulate the experiments of a hydrazine arcjet by Bufton and Burton [1]. Here the thruster has an area ratio of 225:1 and a half angle of 20 deg, with constrictor diameter of 0.64 mm. Hydrazine was simulated as a mixture of 1:2 molar ratio of gaseous nitrogen and hydrogen. The flow rate of the gas mixture is set to 50 mg/s and the input arc current to the thruster was fixed at 10 A. In the experiments of Bufton and Burton [1], a spatially resolved time-of-flight electrostatic probe method was used to measure the radial profiles of axial velocity of gas mixture plasma at 1.0 mm downstream from the exit plane. One can note from from Fig. 2(a) that the predicted axial velocity profile is in good

agreement with the corresponding experimental data. Figure 2b compares the predicted radial distributions of the heavy-species temperature at the arcjet exit plane with the corresponding experimental data of Bufton and Burton [1].Note here that experimental temperature is obtained by indirect means and has large error bars. The predicted temperature however, seems to correctly predict the trend.

G. Simulation results of the hydrazine arcjet

First simulation was carried out for the base case with thruster dimensions as indicated in the upper sub figure of Fig. 1. The mesh distribution is shown in lower sub figure of Fig. 1. The input current was 10 A and hydrazine (emulated as 1:2 mixture of N_2 and H_2) at 4 atm and 500 K enters the thruster. Initially simulation was made assuming entire or full CD nozzle as anode (i.e. convergent section constrictor and divergent section). The converged solution showed that current from anode starts flowing towards cathode in the convergent part of the thruster and up to about first quarter of constrictor region. In the experiments electric discharge is seen to originate in the divergent part and culminates at cathode tip. Several simulations were carried out (by varying the upstream inlet pressure, altering the electrical conductivity to try pushing arc starting location to the divergent side of the thruster. However, these attempts were not successful. From the literature [4-7] it was noted that anode boundary condition applied only on the divergent part or starting from the constrictor. Therefore, rests of the simulations were carried out with anode boundary condition applied on the divergent side only. Figure 3 shows close up of electric discharge region, from cathode tip to anode where arc originates. Figure 3(a) shows the case of full anode (entire CD

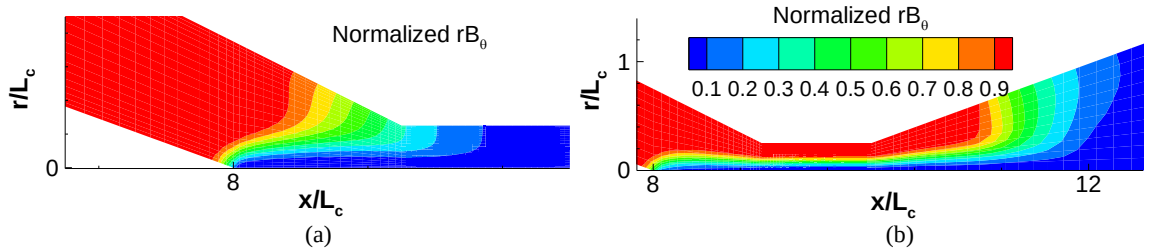

(a) (b)

Figure 3. Normalized contours of rB_θ indicate of current flowing from anode to cathode. (a) full anode (b) anode restricted to the divergent part only. Input current is 10A and inlet pressure of hydrazine is 4 atm and temperature 500 K.

nozzle) and Fig. 3 (b) shows the case of half anode (or where anode is restricted to divergent section only). While electric discharge is confined to convergent section in the former case, the arc originating at divergent part of anode traverses along constrictor to the cathode tip.

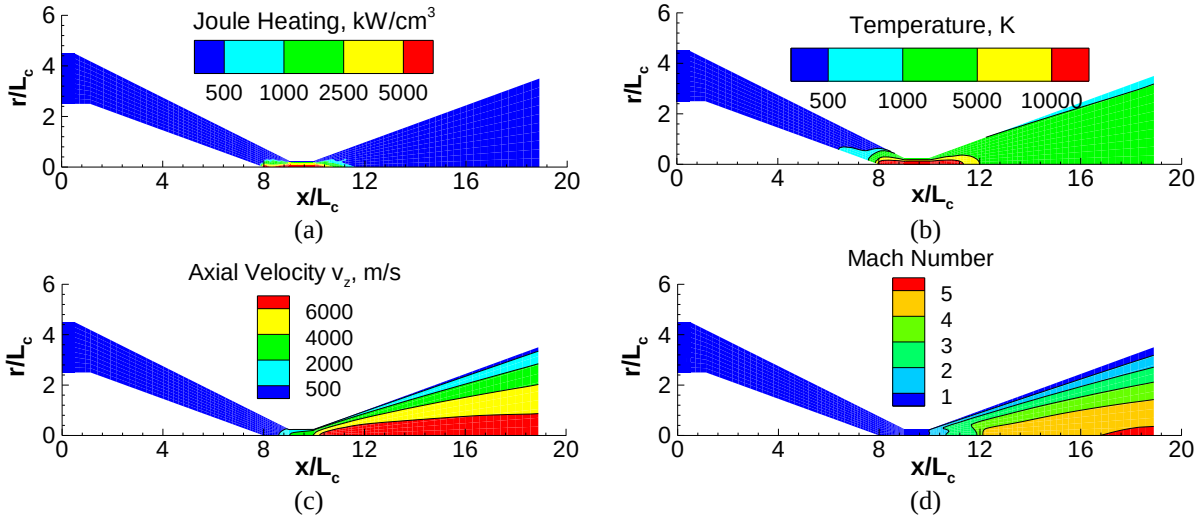

Figure 4. Contours of (a) Joule heating (b) temperature (c) Mach number and (d) axial velocity for hydrazine arcjet operating at input current of 10 A, inlet pressure is 4 atm and inlet temperature is 500 K.

The contour plots of other field variables (for half anode case) are shown in Fig. 4. Figure 4(a) shows joule heating in W/cm3. One can note that heating intensity is higher near cathode tip along the axis along the constrictor length where current density is higher. Consequently the plasma temperature is higher in the corresponding region. The heated plasma expands in the divergent section resulting in decrease in temperature and increase in axial velocity (Fig. 4(c)) and local flow Mach number (Fig. 4(d)).

Next a parametric study is carried out to examine the influence of input current and geometrical design parameters such as constrictor length, cathode length and constrictor radius on thruster performance. The effect of input current on the performance of hydrazine arcjet thrusts for the base geometry is presented in table 1. Simulation results for three different arc currents, 5, 10 and 15 A for inlet stagnant pressure of 4.0 atm and inlet temperature of 500 K are shown in the table. Since stagnation pressure is prescribed the mass flow rate of hydrazine varies depending upon the joule heating inside the thruster. Higher joule heating results in lowering of hydrazine inlet mass flowrate. The joule heating increases with increase in input current and so dos the power required. The specific impulse as expected is seen to increase with increase in input current. However, total thrust developed by the thruster decreases with increase in input current, due to decrease inlet mass flow rate.

Table 1, Thruster performance for various input current

Input Current (A)	Flow Rate (mg/s)	Thrust (mN)	Specific Impulse (s)	Joule Heating (W)
5	20.1	86.4	437	128.4
10	17.1	75.5	476	230.2
15	15.6	72.6	479	266.4

The influence of cathode length on thruster performance is presented in table.2. The cathode length is varied from 7.5 L_c to 9L_c. For all the simulations here input conditions are same as that of the base case where the input current is 10 A, inlet stagnation pressure fixed at 4.0 atm and inlet temperature is 500K. One can note that cathode length (which influences distance between cathode tip and constrictor beginning) does not seem to have much influence on thruster performance; the specific impulse remains nearly the same. It is also noted that joule heating increases as the gap between cathode tip and constrictor start location increases (shorter cathode length), however this does not seem to affect the specific impulse. This may be due to combined effect of change in nozzle area ratio and heat loss.

Table 2, Influence of cathode length on thruster performance

Cathode Length (L_c)	Flow Rate (mg/s)	Thrust (mN)	Specific Impulse (s)	Joule Heating (W)
7.5L_c	17.2	70.4	476	264.3
8.0L_c	17.1	75.5	476	230.2
9.0L_c	17.1	81.1	477	224.2

Simulations were carried out with two additional constrictor lengths, one halved and second increased by 50%. The results of computation are presented in table.3. The input conditions same as for the base case. From the simulation results it is observed that the change in constrictor length over the range doesn't affect the specific impulse. The Joule heating is higher by 25% for longer constrictor. However this does not affect specific impulse, probably due to higher heat loss at the constrictor.

Table 3, Influence of constrictor length on thruster performance

Constrictor Length (L_c)	Flow Rate (mg/s)	Thrust (mN)	Specific Impulse (s)	Joule Heating (W)
0.5L_c	18.4	85.6	474	197.9
L_c	17.1	75.5	476	230.2
1.5L_c	16.5	77.2	477	247.3

The influence of constrictor radius is reported next. Table.4 presents the change in constrictor radius at input current of 10A, inlet stagnation pressure of 4.0 atm and inlet temperature of 500K. The constrictor radius is varied from 0.25 L_c to 0.5 L_c. It is interesting to note that the specific impulse attains a maximum at about 0.35 L_c for the

Table 4, Influence of constrictor radius on thruster performance

Constrictor Radius (R_c)	Flow Rate (mg/s)	Thrust (mN)	Specific Impulse (s)	Joule Heating (W)
$0.25L_c$	17.1	75.5	476	230.2
$0.30L_c$	26.5	126.7	487	233.3
$0.35L_c$	38.7	196.9	517	245.2
$0.40L_c$	54.8	270.1	503	248.6
$0.50L_c$	153.4	629.0	417	489.3

given input conditions and other geometric parameters remaining the same. As the constrictor radius increases the mass flow rate increases, however, the joule heating does not increase as steeply as mass flow rate and thus a non-monotonic trend in specific impulse. The total thrust keeps increasing over the present range of constrictor radii.

IV. Conclusion

A 2D axisymmetric numerical model was developed to simulate hydrazine arcjet thruster. The model was validated in several steps and finally validated against experimental arcjet data available in the literature. The present model assumes chemical and thermal equilibrium thus assume plasma to be single fluid and does not require ionization reactions to be solved for. Instead closer to reality, transport properties are obtained from equilibrium data of Mruphy [8]. The model also includes radiative cooling of anode wall as boundary condition, thus realistic wall temperature distribution can be predicted. The model was used to predict radiatively cooled 0.1 N class hydrazine arcjet thruster. The full anode wall model by default resulted in discharge arc located inside the convergent part of the arc jet. To avoid this unrealistic outcome, anode boundary condition was prescribed on the divergent part of the thruster wall. This resulted in realistic prediction of discharge arc travelling from divergent wall (anode) through the constrictor to the cathode tip. A parametric study was carried to study the influence of geometric parameters and input current on thruster performance. For a given stagnation condition at the inlet, increase in input current increased specific impulse of the thruster, but decreased total thrust. This was due to reduction in propellant mass flow rate resulting from increased discharge arc heating. The geometric parametric study showed that thruster performance was not influenced much by constrictor length and position of cathode. However, influence of constrictor radius was found to be significant. In fact the specific impulse of hydrazine arcjet was found to be maximum for constrictor radius of 0.35 L_c.

Appendix

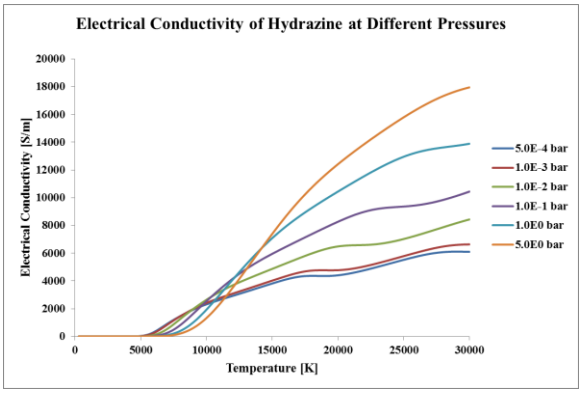

Figure A1 Electrical conductivity of hydrazine plasma

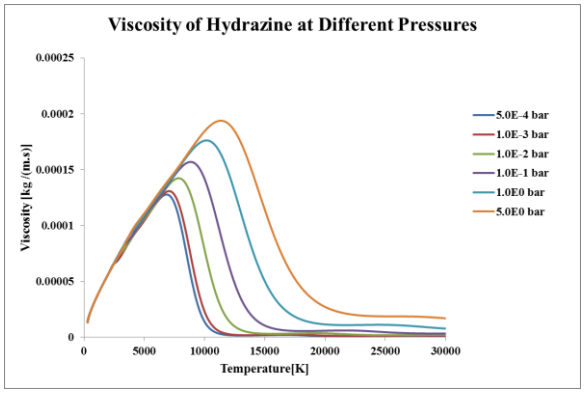

Figure A2. Viscosity of hydrazine plasma

The transport properties of hydrazine plasma were obtained from the work of Murphy [8]. Figure A1, A2 and A3 show plots of electrical conductivity, viscosity and thermal conductivity with temperature at various pressures respectively. To incorporate variation of these properties with temperature and pressure, piece wise polynomials spanning over certain temperature range, with six coefficients were fitted to data for each pressure. These polynomials were used in the CFD code to obtain local properties in the thruster.

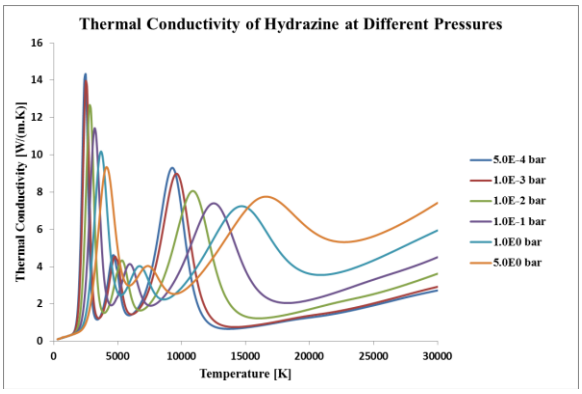

Figure A3. Thermal conductivity of hydrazine plasma

Acknowledgments

The present work was made possible through sponsored research sanctioned by JPC of ISRO-IITM STC for the period 2015-2017.

References

1. Bufton, S. A., and Burton, R. L.,"Velocity and Temperature Measurements in a Low-Power Hydrazine Arcjet," Journal of Propulsion and Power, Vol. 13, No. 6, 1997, pp. 768–774.
2. V. Babu, S. M. Aithal and V. V. Subramaniam "*Numerical Simulation of a Hydrogen Arcjet*" Journal Propulsion Power Vol. 12, No. 6, Nov-Dec 1996
3. Ken-ichi Tanaka and Kazuo Tsuchiya "*Computational Investigation On The Characteristics Of A Low Power DC Arcjet Thruster*" IEPC-93-82 754
4. Hai-Xing Wang, Shao-Xia Jia , Xi Chen and Wenxia Pan "*Two-Dimensional LTE Modeling of a Low-Power Argon Arcjet Thruster*" IEPC-2009-258.
5. Hai-Xing Wang, Jin-Yue Geng, Xi Chen, Wenxia Pan, "*Numerical Simulation of a Low-Power Hydrazine Arcjet Thruster*" Physics procedia Vol. 32, P732-742, 2012
6. Yan-Ming Wei, Qing-Song He and Hai-Xing Wang, "*Chemical Non-equilibrium Modeling of Low-Power Nitrogen/Hydrogen Arcjet Thrusters*" Journal Propulsion Power Vol. 32, No. 6, P1472-1482 2016
7. Qingsong HE and Hai-Xing Wang, "*Non-equilibrium modeling study on plasma flow features in a low-power nitrogen/hydrogen arcjet thruster*" Plasma Sceince and technology, Vol. 19. No. 5, 2017.
8. Anthony B Murphy, "*Transport coefficients of plasmas in mixtures of nitrogen and hydrogen*" Journal Chemical Physics Vol 398, No. 1, P67-72, 2011